HHS Public Access

Author manuscript

Appl Mater Today. Author manuscript; available in PMC 2020 September 01.

Published in final edited form as:

Appl Mater Today. 2020 September ; 20: . doi:10.1016/j.apmt.2020.100752.

3D Printing metamaterials towards tissue engineering

Elvan Dogan[a], **Anant Bhusal**[a], **Berivan Cecen**[b], **Amir K. Miri**[a,c,*]

[a]Biofabrication Lab, Department of Mechanical Engineering, Rowan University, Glassboro, NJ 08028, United States

[b]Division of Engineering in Medicine, Department of Medicine, Brigham and Women's Hospital, Harvard Medical School, Cambridge, MA 02139, United States

[c]School of Medical Engineering, Science, and Health, Rowan University, Camden, NJ 08103, United States

Abstract

The rapid growth and disruptive potentials of three-dimensional (3D) printing demand further research for addressing fundamental fabrication concepts and enabling engineers to realize the capabilities of 3D printing technologies. There is a trend to use these capabilities to develop materials that derive some of their properties via their structural organization rather than their intrinsic constituents, sometimes referred to as mechanical metamaterials. Such materials show qualitatively different mechanical behaviors despite using the same material composition, such as ultra-lightweight, super-elastic, and auxetic structures. In this work, we review current advancements in the design and fabrication of multi-scale advanced structures with properties heretofore unseen in well-established materials. We classify the fabrication methods as conventional methods, additive manufacturing techniques, and 4D printing. Following a comprehensive comparison of different fabrication methods, we suggest some guidelines on the selection of fabrication parameters to construct meta-biomaterials for tissue engineering. The parameters include multi-material capacity, fabrication resolution, prototyping speed, and biological compatibility.

Keywords

Metamaterials; Additive manufacturing; Multiscale; Tissue engineering; Bioprinting

1. Introduction

Mechanical metamaterials have been designed to display counterintuitive physical behaviors [1], negative elastic modulus [2], negative Poisson's ratio [3], and other unusual constitutive behaviors [4]. The inspirations were taken from human ingenuity, mathematical inventions, and sometimes nature to create novel structures possessing unconventional capacities. The class of such materials, referred to as metamaterials, was started with porous implants [5],

*Corresponding author. miri@rowan.edu (A.K. Miri).

Declaration of Competing Interest

No conflict of interest declared.

which includes biomimetic materials created by nature-derived architectures. Mechanical metamaterials have also offered radical designs of functional tissue scaffolds [6], showing promising potential in bone tissue regeneration and orthopedic implants [7], possessing capabilities such as extreme stiffness-to-weight ratio [8], tunable hydraulic permeability [9], and even high surface-to-volume ratio [10]. The physical properties of meta-biomaterials are regulated by the design of underlying microstructure [11]: for example, the characteristics of natural materials such as wood and nacre have been applied to design hard tissue substitutes. Metamaterials have been recently proposed to supplement implants and tissue scaffolds for other organs [12], but achieving the application of novel microarchitectures in functioning prototypes is limited by the scalability of current manufacturing methods [13].

Current imaging and analytical tools can be used to reveal ordered structures on multiple length scales and to illustrate how each hierarchy contributes to the resultant bulk material properties [13]. This process has been used to understand the structure-function relations in biological tissue structures [14,15]. One established example is trabecular bone, which has a hierarchical layout of porous or cellular architectures distributed through seven orders of magnitude in length scales [16]. The mesoscale porous structure is comprised of a network of ligaments, each of which contains a complex architecture consisting of a network of microstructural hollow fibers, each composed of concentric lamellae at the submicrometer level. This hierarchy contributes to the high strength and fracture resistance. As another example, the viscoelastic dermis partially undergoes partially dissipation through viscous sliding of underlying collagen fibrils for remodeling, and the elastic behavior of skin tissue is critical in the post-deformation shape recovery [17]. The dermis has a low stiffness region at small strains and an increased stiffness at large strains under mechanical deformation [17,18]. The elastin fibers provide elasticity and softness at low strains; thus, the skin becomes mechanically stiff in deformation above a pre-defined stretching strain and can be protected from failure under large strains. Biomimetic human skin tissues are in demand in the current market of soft electronics [19]. Stretchable electronics must meet the requirements for bending, twisting, stretching, and deforming into complex curvilinear shapes [20]. The self-limiting properties of skin should also be employed in a stretchable substrate or flexible device, in which the level of device performance is preserved in response to large deformations. Another example is the engineering of cartilaginous tissue, which depends on the relationship between chondrocyte response and the physical properties of the scaffold, namely the gradient of stiffness, hydrophilicity, and deformability. Mechanical stimulation associated with normal body functions is crucial in modulating engineered articular cartilage [21]. Chondrocyte proliferation in an auxetic polymer was studied under compressive stimulation for cartilage regeneration [22]. The isotropic compressive load onto the cells was assumed to lead to a higher rate of proliferation. Current three-dimensional (3D) printing technologies can be more beneficial in fabricating structures with superior resolutions when compared to classical methods [23]. Table 1 summarizes the current trend of fabrication methods with outlooks in designing new structures.

The objective of this review is to study current techniques in fabricating desired meso- and micro-structures in mechanical metamaterials. The theoretical background or niche behind each pattern or structure is outside of the scope of this paper, instead looking more at the fabrication and practical standpoints. We have divided the fabrication methods into three

main groupings: conventional, light-assisted, and extrusion-based additive manufacturing (AM) methods (see summary in Table 1). Light-assisted AM involves transferring the ink onto a substrate by light energy or crosslinking the ink by light-material interactions. Extrusion-based AM uses direct contact between a deposition substrate and the printhead from which the ink is deposited, normally with a sufficiently high pressure to ensure ink transfer onto the substrate. These approaches each have their own merits and shortcomings, depending on the desired application of the structure. We discuss the limitations of each technique for creating metamaterial structures and project the trend of AM techniques toward advanced structures in biomedical engineering. We hope that this review may help researchers to select and customize efficient 3D printing methods and design strategies for biomedical metamaterials.

2. Mechanical metamaterials

Conventional fabrication methods involve the use of casting and machining tools for metals and the use of injection molding technologies for plastic and polymer materials. Researchers initially applied plastics and polymer-based materials for making new structures based on cost, material flexibility, and machinability of polymer materials. Modular and reconfigurable structures and some of the prototypes built by architects are examples of classical routes to fabricate, usually large scale, metamaterials. Mother Nature is a unique conventional pioneer in creating highly ordered, multi-scale architectures; however, conventional methods are limited and are not tailorable for developing personalized metamaterials. The design of multi-scale natural constructs could pave the way for developing technologies toward synthetic and tunable metamaterials.

2.1. Ultra-stiff materials

Many natural materials have staggered microstructures and show superior mechanical properties such as strength, toughness, and stiffness [85]. Stiffness-related elastic constants include the elastic (Young's) modulus, shear modulus, and bulk modulus [86]. Cellular metamaterials are inspired by nature and identified by their uniqueness in stiffness [87], mechanical toughness [88], ultralightness [89], and strength resistance across various length scales [90]. The main intention in introducing hierarchy to cellular structures is to improve the stiffness-to-weight ratio, and a honeycomb structure has been the most popular design [91]. Kooistra et al. designed a hierarchical honeycomb where the homogeneous unit cell walls were replaced by elastic trusses [24]. Apart from a brick-and-mortar arrangement, inspired architectures from nacre are of interest as they exhibit both appealing hierarchical structures and remarkable mechanical properties [26]. Composite origami was also introduced by storing Tachi-Miura-Polyhedra in a flat state and deploying to a finite volume with defined axial stiffness, while polyurethane resin was then infused to hold the structure together [25]. It was shown that the stiffness is highly tunable and dependent on several geometric properties as well as the material properties of the crease-lines. The process is a labor-intensive manual process, and for small and large scale manufacturing folding becomes increasingly complex [27]. There are other methods for composite origami structures, one of which is kirigami, a manufacturing technique relying on creating cuts in the folding pattern before having a volumetric structure [28]. Another example is a pre-

folded honeycomb as a high-performance energy-absorbing structure (Fig. 1Ai). A conventional aluminum honeycomb base was folded through a Miura origami pattern, in which the structural strength of the pre-folded honeycomb was significantly higher for in-plane direction than that of conventional honeycomb (Fig. 1Aii) [30]. Similarly, Victrex PEEK polymer sheets were used to form different types of honeycomb structures (e.g., closed, open) through a Kirigami technique consisted of folding operations for making a 2D sheet material into a 3D cellular structure (Fig. 1Aii). They also employed finite element analysis to show that such open and (traditional) closed honeycomb structures displayed significantly different mechanical behaviors from each other [31]. Such a method preserves the foldability of structures and repeatability of geometric shapes [29].

2.2. Auxetic materials

Poisson's ratio represents the relationship between the transverse and longitudinal strains under uniaxial loading, and it falls between 0 and 1 for engineering and natural materials. Engineers have proposed radical designs with negative Poisson's ratio, known as auxetics. Auxetic materials are characterized by lateral expansion when stretched (in contrast to conventional materials) [67]. Since 1980s, structural variations have been used to manufacture irregular structures [92]. Auxetic structures were formed by making a re-entrant unit cell using one-stage volumetric compression, which experienced long-term stability and was able to revert to the original structure [55]. Later, foam blocks were fabricated using multi-stage processing techniques, such as variations in volumetric compression ratio and temperature, to minimize surface creasing and control Poisson's ratio [50]. Some suggested quasi tri-axial compression (Fig. 1B) [166]; for example, it was used for polyurethane, yielding maximum reentrancy of −0.27 and −0.31 with enhanced rigidity and improved isotropic behavior when compared to its parents [51]. As another approach, auxetic fibers with diameters of less than 1 mm were produced by melt-spinning of polypropylene [52]. These fibers could be used to produce an auxetic fiber-reinforced composite by altering the stacking sequence to produce a negative Poisson's ratio throughout the material thickness [53]. An auxetic material can be used as a piezoelectric sensor due to it increasing the sensitivity of the device. Milton map represents bulk modulus vs. shear modulus for different Poisson's ratio [57]. In general, auxetic materials can be either polymers or metals. The first auxetic polymer material was based on polytetrafluoroethylene [54], followed by other polymers such as high molecular weight polyethylene [93], polypropylene [94], and Nylon [95]. Re-entrant copper foam is among the first reported auxetic metals, in which it was fabricated by the application of small increments in plastic deformation along orthogonal directions (leading to Poisson's ratio ~ −0.39) [55]. The foam was prepared by permanent sequential compression to achieve a triaxial compression where Poisson's ratio was −0.8, while toughness was increased by annealing [56].

2.3. Super-elastic materials

Super-elastic materials are those which reversibly deform to a high strain in response to high stress. These can be categorized as metallic and non-metallic [85]. Metallic materials are often resistant to corrosion and deform when a voltage or heat or similar physical conditions are applied. The tribological aspect of superelastic alloys is a key component in their applications. An example is copper-aluminum-nickel with 14% weight aluminum, and 4%

weight nickel [96]: this alloy can either be mono-crystalline or poly-crystalline. In addition to modified metals, microstructural variations of other classes of materials may impose superelastic properties. Carbon can lead to super-elastic materials under a lamellar multi-arch design for the crystal structure (i.e., carbon-graphene). It showed high fatigue resistance, compressibility, as well as super-elastic properties [57]. When combined with carbon's lightweight and conductive properties, non-traditional applications can be considered for the future. Another useful form of carbon is graphene. The nano-ribbon forms of graphene can be integrated into rubber materials such as polydimethylsiloxane (PDMS) to make a lightweight, super-elastic strain electronics [54]. Specific parameters can be changed such as geometrical configuration, restrains of the PDMS, and size of the ribbons (Fig. 1C). A mainstream of super-elastic devices is in electronic devices and the scalable aspect of this process combined with biocompatibility of the sensor can lead to its implantation. Super-elastic materials are used in a wide range of fields.

2.4. Self-assembly and programmable materials

Nature has inspired new material designs which respond to external stimuli in a controllable and predictable manner [97]. Self-assembly processes involve particles arranging themselves in a systematic structure, and programmable materials shift from one shape to a pre-memorized shape-changing condition (defined by shape-shifting pathways). Self-assembly can be active or passive [98], where passive materials interact according to geometry, surface chemistry, and intermolecular forces for thermodynamic equilibrium and active material particles interact according to predesigned programs among components. One of the extensively studied materials is a class of polymers known as smart polymers or stimuli-responsive polymers [99]. A bilayer thermo-responsive polymer from PDMS-gold and PDMS-silicon carbide composites was made by a combination of casting, molding, and sputter coating [70]. An origami-inspired technique to transform 2D objects to 3D objects was used to self-fold the hinges to create complex geometries based on a thermo-responsive shape memory polymer [71]. A similar method was applied to fold a pre-strained polystyrene sheet using a dark ink pattern at the hinges to absorb the heat from infrared light above the glass transition temperature to change the shape [72]. Electrospinning can also be used to manufacture a temperature-sensitive combination of soft and elastomeric using poly (ε-caprolactone) and silicone rubber (Fig. 1D) [73]. The human body has a different condition such as variable pH and temperature, so these materials can be used as the implants. Additionally, targeted drug delivery can be enabled using self-assembly and programmable materials, using stimuli from within the human body to trigger a response [74].

3. Light-Assisted additive manufacturing of metamaterials

Commercially-available light-assisted techniques use a similar strategy: exposing a liquid-like ink to focused light beams, resulting in ink solidification. The techniques may differ based on the light wavelength, light excitation, and mechanism of ink feeding. Laser beams or collimated light sources are normally used for light generationwhile galvanometers or micro-mirror devices can be used for directing and focusing the generated light. Vat polymerization, powder-bed fusion, or directed energy deposition technologies are then used

to induce the material fabrication process. The inks range from metals, ceramics, polymers, and composites to multi-component medical materials [100]. Light-based AM processes follow similar principles, though differences in materials arise by their interactions with light [101]. A thermal energy source is commonly used for sintering, or melting and consolidation of the powder material, while a light source is used for photocrosslinking of the liquid-based inks during vat photopolymerization [102]. Two popular techniques in the category for metal-based inks are selective laser sintering/melting (SLS/M; based on a powder-bed) and laser engineered net shaping (LENS; based on a blown-powder) which both use powder-based materials, and a less-common technique is laminated object manufacturing (based on a metallic foil) [103–105]. For the case of polymers and plastics, stereolithography (SLA) and digital light processing (DLP)-based SLA have been proposed to offer advanced fabrication methods [106]. Most of the methods reviewed here are not very effective in achieving resolutions of better than 50 μm resolution to fabricate 3D structures for mechanical metamaterials [107]. To tackle this problem, direct laser writing, deep ultraviolet (UV) lithography, electron/ion beam lithography, and nanoimprint lithography have been proposed by researchers [76,108–112]]. Two-photon absorption (TPA) that can reach resolutions down to 200 nm was proposed originated from multi-photon imaging techniques [107,112]. In this section, we summarize different classes of metamaterials such as auxetics [113,114], self-assembly [114,115], ultra-stiff [59,114], and super-elastic materials [114,116] exhibiting tailored and multifunctional properties [32,36].

3.1. Selective laser sintering/melting

The SLS process involves the deposition of a predefined, thin layer of material powder onto a substrate controlled by a roller that can move along the vertical direction. A laser beam, guided by Galvano mirrors, selectively moves above the surface covered by the powder, and the interaction of light and material powder sinters the particles. Un-sintered powders will provide mechanical support and avoid the collapse of the solidified structure. Following the sintering step, the surface will be lowered down to one layer thickness, ranging between 20 and 100 μm. Another thin layer of material powder is deposited on the surface, and the cycle repeats until the desired 3D structure is formed while an inert gas (e.g., nitrogen, carbon dioxide, or argon) is flowed through the set-up to prevent powder oxidation during the sintering process (Fig. 2Ai–ii) [39,105]**.** Despite the LBM method, the powder does not necessarily melt throughout the SLS process. Because SLS is a semi-solid phenomenon, the fused solid-phase particles exhibit high porosity, which leads to undesired surface roughness (i.e., poor surface quality) and low tensile strength in fabricated parts [117,118].

Yuan et al. [63] fabricated soft auxetic lattice structures using SLS while considering the evaluation of physical and thermal properties of highly porous thermoplastic polyurethane powder to particularly explore the potential of manufactured auxetic lattice structures for energy absorption. The proposed soft polyurethane auxetic lattices were capable of withstanding cyclic large deformations with negative Poisson’s ratio. Tailorable and flexible 3D soft metamaterials were made by using polyurethane powders and optimizing the processing parameters, such as laser power and scanning speed. In a different work, tetrarchical and anti-tetrarchical hybrid chiral stent samples made of SS316LN stainless steel alloy with auxetic properties have been fabricated with the SLS technique [58]. Finite

element analysis and *in situ* uniaxial compression were used to demonstrate the auxetic response of the stent structure in action.

Both SLM and SLS processes are similar, and the key difference comes from the laser types. In contrast to SLS, a laser of higher energy is used to melt the powder in SLM, which can result in superior mechanical properties [119]. The SLM-based parts have metallurgically bonded structures that possess high densities, enhanced mechanical properties, and fewer post-treatment procedures compared to SLS [120]. An unmodified SLM was used to fabricate composite structures made of polymer powders, metal-coated, and pre-alloyed powder. Laumer et al. [37] demonstrated a compatibility matrix for possible combinations of polymers that are used for fabricating composite structures. They also showed the difference between layer coatings using coated powders with pre-alloyed powders in terms of homogeneity of the coating, which also directly affects the tensile properties. In another work, a multi-functional structure was made through SLM to create an auxetic TiNi (shape memory alloy)-based armor [59]. The effects of SLM process parameters such as laser power, scan speed, and tracking rate on the structural integrity of structures were also studied. Ding et al. [60] used a robotized laser-based metal AM for making complex metal structures, low-volume manufacturing, and high-value component repair or modification. They made a rhomboid shape auxetic structure to assemble a metallic structure with a Poisson's ratio of −0.8 (under tensile load and ~20% strain).

3.2. Laser engineered net shaping

LENS (Fig. 2Bi) uses a nozzle-based powder delivery system, which allows mixing two or more different metal powders that can include stainless steels, titanium alloys, tungsten, copper, and aluminum. The spatial resolution is limited by the laser size rather than the powder particle size [121]. Simultaneous interactions of the powder stream and high-power laser beam (ranging from 0.5 to 4 kW) along with an inert gas acting as a shield will form the desired pattern [122]. Antolok-Dudka et al. fabricated a titanium allow (Ti6Al4V) thin-walled honeycomb structure with a thickness of 0.7 mm (ultra-stiff). They used computed tomography (CT) data to assess the metallurgical quality for the honeycomb-shaped structures before and after sandblasting. Before and after sandblasting samples, the surface roughness was found to be independent of the unit cell size (Fig. 2Bii–iv) [32]. This may indicate that the LENS technique eliminates the need for post-processing, resulting in fabricated parts possessing low geometric tolerances that are suitable for use in medical applications.

The LENS process suffers from several production issues, such as porosity, crack formation, and premature fusion [123]. The quality of the fabricated part depends on the surrounding environment and on cumulative heat effects during the material deposition process [123]. Study of the molten pool temperature may help identify the thermally-induced defects during the material building process. Other inherent drawbacks include poor surface finish, slow deposition rate, and low fabrication precision [124]. These problems can be addressed by adjusting process parameters and utilizing other techniques such as the production of near-net shaped components, easier control of the matrix structure, and use of a wide variety of materials [125] Being able to better control of the powder quantity, laser power, working

space, and focusing conditions in LENS may lead to an advanced tool for the microstructure development in metamaterials.

3.3. Stereolithography

SLA involves a photo-polymerization process which creates patterns layer-by-layer. This is achieved by shining ultraviolet light with a defined wavelength onto photosensitive liquid monomers to form a crosslinked structure [126]. A typical ink for such a process is a suspension of photocurable acrylic resins mixed with microparticles and powders, while the obtained structure is then post-processed to eliminate any phase of the additives. The SLA technique has become a popular choice for creating metamaterials. For example, Pandini et al. printed a shape memory polymer-based auxetic structure with a Poisson's ratio of − 0.18 using SLA, using a 405 nm UV laser and a commercial photopolymer resin (FLGPCL02) with a broad glass transition interval. They created this printed auxetic structure to obtain thermally-triggered hierarchical motions and self-deployment capabilities [62]. Zarek et al. printed shape memory objects which can be specifically applied in soft robotics (i.e., self-assembly), minimally invasive medical devices, and wearable electronics combining conductive materials and methacrylated polycaprolactone (PCL) with a modified SLA, inkjet-based printer [75]. Another class of metamaterials is for optical purposes (sometimes not considered to be mechanical metamaterials). Sadeqi et al. fabricated high-frequency optical absorbers using a novel mushroom-like geometry and a hybrid approach consisting of SLA printing, metal coating, and wet etching. They used a photopolymer resin to print metamaterial patterns with a radius of 500 μm and unit cell size around 2 mm, and after 3D printing, metal coating, and etching with some surface modifications have been performed [76]. In another work, Mohsenizadeh et al. fabricated a stretching-dominated lattice structure with enhanced energy-absorbing ability [68]. They used a photopolymer resin to print octet-truss unit cells with 500 μm solid circular cross-sectional elements to form an overall lattice structure through an inverted SLA printer. The fabricated structure exhibited an almost complete recovery after multiple compression tests under 70% strain and 8–11% higher energy absorption efficiency compared to both expanded polystyrene and Duocel aluminum foams.

3.4. Digital light processing

The digital light processing (DLP) technique was developed through the modification of SLA by incorporating digital micromirror chips that make a single layer to be patterned by light projection [127]. DLP technique provides a faster and more efficient photo-polymerization process at a wider range of wavelengths compared to SLA printing [128]. The DLP printing resolution is directly dependent on the pixel size of the micro-mirror chips and their distance from the optical window [129], with the highest achievable printing resolution for DLP technique was reported to be 10 μm. A customized DLP printer using an objective lens was developed to reduce the smallest pixel size [130]. This technique is capable of printing a 3D structure with resolutions better than SLA.

Sometimes called projection micro-stereolithography (PμSL), DLP can be used to make 3D structures with a very low thickness in each layer (down to 1 μm). PμSL makes it possible to readily produce ultra-light and ultra-stiff metamaterials, with a wide range of material

options (polymers, metals, or ceramics), combined with nanoscale coating and post-processing [33]. Sun et al. fabricated a small structure with ~ 0.6 μm resolution. It is possible to fabricate metallic and ceramic high-resolution micro-lattice structures through post-processing printing polymer parts such as nano-coating [34], thus the variety of materials to work with is wider than for other optical techniques [34], and DLP-based methods can polymerize entire cross-section in a single exposure projecting UV light through a high-quality digital mask [107].

Zheng et al. fabricated ultra-stiff metallic structure with hybrid hierarchical topology possessing thin-walled hollow tubes and a thickness ranging from 50 to 700 nm at the lowest hierarchy through PμSL [13]. The nickel-phosphorus metamaterial exhibited both super-elastic tensile (up to 20% strain) and high compressive elastic deformation (up to 50% strain) behavior with ultra-low density (Fig. 2Ci–ii). In another study, multi-material thermal responsive, shape memory polymer structures were made using methacrylate-based polymer resin at different compositions (Fig. 2Ciii) . The manufacturing was enhanced through an integrated material exchanging mechanism incorporated into a PμSL system [77]. Later, a customized, compact LED-based PμSL printer was used to print mesoscale structures with microscale features [35]. Microstructures with 1 μm layer thickness were fabricated using a photopolymer resin composed of acrylate-based commercial monomers. Another study reported the fabrication of multimaterial auxetic lattice structures were fabricated by a robotic multi-material PμSL and varying stiffness through control over the resin mixing. The modified system allowed integrating multiple materials such as monomer resins with functional nanoparticles and various cross-linking degrees [64].

3.5. Flashing photopolymerization method

This novel light-assisted 3D printing method was developed to improve the printing resolution through reducing scattering. The system uses a xenon flash tube as the light source, which is connected to an electronically triggered controller unit. Using an optical lens, a digital micro-mirror device projects the photomask image onto and through a transparent anti-adhesion substrate made of PDMS [41]. In the flashing photo-polymerization method, light exposure is delivered discontinuously by millisecond flashes, reducing the light scattering and thus improving the resolution. Three governing factors in optical scattering are the size of the molecules, degree of crystallinity, and phase separation. Homogeneous polymer material can cause Rayleigh scattering (scattering from molecules and tiny particles of diameters less than 1/10 wavelength). Phase separation can also cause decreased homogeneity that increases the degree of light scattering. You et al. have developed this method for 3D printing and successfully printed optically clear polymer material with higher resolution compared to using a continuous photo-polymerization technique [41].

3.6. Two-Photon absorption

Two-photon absorption (TPA) is a promising technique for high-resolution 3D printing that can fabricate arbitrary and ultraprecise 3D structures with resolution of less than 100 μm (as low as 30 μm), such as micro/nanophotonics, microfluidics, drug delivery devices, transdermal needles, and bioimplants [40,131–133]. In TPA, a single femtosecond-pulsed

laser source is used for the photopolymerization reaction in which a photoinitiator absorbs two low-energy photons simultaneously near the infrared spectrum. Photopolymerization can occur within any 3D spatial positions in a substrate according to the CAD model, which makes it possible to eliminate the necessity of supporting material (Fig. 2Dii) [40] in contrast to conventional SLA technique in which polymerization is limited to only the surface of the printing area [107,126]. Moreover, the short-wavelength UV light used in SLA may cause photochemical damage to biological tissue, while near-infrared (NIR) spectrum light source used in TPA enables fabrication of photo-polymerized 3D structures in the presence of cells. This makes TPA an attractive technique for bioprinting of drug-delivery systems, microelectromechanical systems (MEMs), and scaffolds for tissue engineering [132,134,135]. Meza et al. fabricated ultra-stiff and energy-absorbing metamaterials made of hierarchical hollow-tube alumina nanolattices composed of nanoscale ceramic through hybrid technique including TPA, atomic layer deposition, and oxygen-plasma etching. They created these structures with wall thicknesses ranging between 5 to 60 nm and with mass densities ranging between 6.3 to 258 kg/cm^3 that can recover their original shape above 50% strain [36].

Obata et al. customized a TPA platform for the fabrication of 3D polymer structures with a high-aspect ratio (Fig. 2Di–ii). Their set-up used a stage that moves the microscope objective, immersion oil, and cover glass into the photosensitive ink, thus providing a higher (up to 7 mm) and wider objective working range. The wider range of the printing area is defined by the overall height beyond the working distance of the microscope objective. They used a mixture of pentaerythritol tetraacrylate and 4,49-bis (diethylamino) benzophenone as the ink [38]. Zhang et al. [61] used TPA technique producing 800 nm central wavelength laser with 1 mm head diameter and 100-femtosecond wide pulses at a repetition rate of 80 MHz with a maximum power of 350 mW to fabricate suspended web structure with tunable Poisson's ratio. They demonstrated mechanobiological cellular behavior differences in web-structured polyethylene glycol-based hydrogels with both negative and positive Poisson's ratios.

3.7. Continuous liquid interface production

Continuous liquid interface production (CLIP) provides high speed (up to 500 mm/h) and nearly-layer-less, smooth construction of structures (down to 1 μm thickness) by injecting oxygen gas into the photopolymerization site to inhibit polymer crosslinking at out-of-focus areas [114]. The oxygen-containing dead zone creates a very thin layer of uncured photosensitive ink between the cured part and bath bed; thus, the structure can be made continuously through moving the holding plate while projecting cross-sectional UV images from the DLP system simultaneously (Fig. 2Ei–ii) [42]. It is thus promising for creating hierarchical metamaterials at high resolutions as well as soft elastic polymers [136,137] and ceramic-embedded polymer resins [138]. For example, Huang et al. fabricated shape memory structures (Fig. 2Eiii) through CLIP using alginate/polyacrylamide hydrogels, which were ionically conductive and sensitive to external forces induced by calcium and iron ions. Thus, CLIP is a promising technique for self-assembly and programmable metamaterials applications [78].

4. Extrusion-based additive manufacturing of metamaterials

In general, extrusion-based methods deposit a viscous paste-like ink through an extruder nozzle in a layer-by-layer fashion. In case of fused deposition modeling (FDM), the ink melts before flowing to the nozzle and solidifies after deposition onto a solid substrate or the preceding layers. The deposited layers are bonded and welded through a thermally-driven diffusion process. This process produces a selective layer-by-layer construction, offering improved design and fabrication flexibility compared to conventional approaches. In this section, we begin by discussing extrusion-based techniques that use single printheads before moving to multi-printhead platforms. While light-assisted methods are suitable for metals and polymers, the extrusion-based methods mainly cover polymer-based and polymer-metal composite metamaterials.

4.1. Single-Nozzle extrusion

Conventional platforms emply a single printhead using inks that range from alloy-based pastes to natural-derived hydrogels [139]. These inks need to possess specific rheological behaviors such as shear thinning. The paste-like ink is extruded out of the nozzle tip at a specific rate. For some applications, the extrusion of the inks can be tailored to shrink the filaments once deposited, resulting in smaller diameters based on shrinkage ratio. Mirzaali et al. used a combination of auxetic, conventional, and transitional unit cells to create soft shape-matching metamaterials [65]. They used FDM to manufacture a PLA-based structure and then subsequently used elastomeric polymers to fabricate the metamaterial for soft robotics and wearable applications. Bodaghi et al. used FDM to create temperature-stimulated self-morphing 4D structures from PLA filaments [69,81]. They conducted experimental and numerical studies on the mechanical behaviors of metamaterials made from hyper-elastic auxetic structures (Fig. 3Biii) under both tension and compression over a large strain range, revealing buckling instability characteristics. In another work, Wang et al. demonstrated very stable dual-material auxetic structures consisting of stiff walls and elastic joints [66]. The numerical simulations and experimental validation confirmed both the distinct auxeticity and physical properties of such structures when compared to conventional single-material auxetic structures. In another study, Garcia et al. [82] designed and fabricated a wholly dielectric uniaxial anisotropic metamaterial, from polycarbonate using FDM. Using classical planar tessellation theory for standard 2D models, Yang et al. looked for configurations for honeycombs of first and second order, systematically investigated the design properties of current auxetic and non-auxetic systems in 2D and 3D. Next, they developed and rated 3D hierarchical metamaterials in terms of the first-order and second-order structures based on topology research, which led to various Poisson’s ratio and Young module ranges [46]. Kim et al. developed an ABAQUS model of a ferromagnetic, self-assembling, auxetic metamaterial (Fig. 3Bi) that responds to magnetic fields by collective bulk stresses. They used a composite ink made of magnetic microparticles (neodymium-iron-boron alloy fumed silica) embedded in a silicone rubber matrix. The matrix included a silicone catalyst and a crosslinker was formed by a single-nozzle direct ink writing method [79]. Similarly, Wickeler et al. [43] fabricated origami-like structural materials with high strength-to-weight ratios that can be used as sandwich structures using PLA and polycarbonate filaments (Fig. 3Bii). They formed a sandwich structure placing the PLA

origami-like metamaterial between two polycarbonate plates to apply compression and impact tests. The elastic compression moduli of both triangular and rectangular patterns were higher than the existing models in the literature.

Recently, wet metal printing was introduced using CoCrFeNi alloy as a backbone, poly-lactic-co-glycolic-acid as binder, dibutyl phthalate as a plasticizer, and ethylene glycol butyl ether as a surfactant [47]. A blend of metal powders consisting of Co_3O_4, Cr_2O_3, Fe_2O_3 and NiO was extruded through FDM. After reduction and sintering, the printed strut diameters of the micro-lattice structure were around 100 μm and demonstrated comparable and even higher strength and ductility at both ambient and cryogenic temperatures compared to cast alloy.

4.2. Multi-Nozzle extrusion

Multi-material processing can facilitate AM with multi-agents and/or metamaterials [140,141]. By continuous operation of dual extrusion nozzles, the printing time can be reduced. The printing time can be reduced by continuous operation of both nozzles of the extruder [4 8,4 9]. More than two nozzles are used by simultaneously feeding several different ultra-stiff and auxetic materials, allowing either multi-color printing or using different metamaterials. Momeni et al. compared the strength and energy storage capability of the four different lattice structures fabricated through FDM with polylactic acid (PLA), PLA as a single material, and a combination of these two materials in interior and exterior unit cells separately as dual-material unit cells. They analyzed in greater depth the vulnerability of the printed polygonal grid to differences in the thickness of internal and external components [45]. An integrated computer vision framework is the core of a low cost and extendable vision-based multi-metamaterial 3D printing platform [142].

Recent research has also used computer graphics in printing models with the desired color [143]. The research community has made many efforts to build multi-material manufacturing platforms. Some scientists have used multiple powders injections [144]. Moreover, powder-based 3D printing makes full-color printing possible [145]. Hardin et al. demonstrated that multi ultra-stiff and auxetic material inkjet-based systems have also been designed specifically for printing with biopolymers and tissue engineering applications [146].

The next frontier of 3D printing is the ability to integrate both form and function into the printed object. They showed the capability of moving beyond prototyping, new auxetic materials, and flexible printing platforms are required [146]. They also demonstrated that viscoelastic inks made of a variety of materials, including ceramic particles, metal particles, polyelectrolytes, hydrogels, filled epoxy resins, and even extracellular matrices, are usable in a promising process known as direct ink writing (Fig. 3Cii) [114,140]. To date, this extrusion-based printing method has been used to fabricate functional devices. This approach to printing was also used for multiple ultra-stiff and auxetic materials, but multi-material architecture often involves the sequential deposition of individual inks with multiple nozzles [48,146]. Recently, a novel multiple printhead that can extrude up to eight different viscoelastic inks was developed [48]. They fabricated seamless Miura origami patterns and soft robotic millipede-like structures through co-printing of multiple epoxy and

silicone elastomer inks in order to vary the stiffness (Fig. 3Di–iii). The disadvantages of printing one substance at a time include the need to carefully align each nozzle and start and stop ink flow [147]. Bodaghi et al. studied the production of one lattice of versatile beams with embedded SMP fibers, organized to a tubular shape to demonstrate one of their possible stent applications. They also developed thermomodels that were used to simulate the finite-structure to determine thermal deformation [84]. The authors created a finite element model that defines 4D printing materials programming.

4.3. Co-Axial extrusion

Objects made of hollow or filled fibers were mainly made with coaxial extrusion nozzles [83,148]. Thermoplastic materials, such as tubular alginate/PCL scaffolds, were made using a coaxial melt-derived printhead as a first trial [83]. Yanqiu et al. designed and fabricated a functional tactile sensor through sacrificial coaxial extrusion AM and PDMS (Fig. 3Ai–vi) [80]. During thermal curing, they used deionized water as the sacrificial substance. Injecting liquid metal ink (75% gallium, 25% indium) into the PDMS tube to create the resistive sensing part, the device was completed with copper wires to test the node resistance of coaxial fiber grids. In another study, a novel hybrid hydroxyapatite/PCL shell/core scaffold was made through robocasting after fabricating the ceramic ink-based shell and paraffin-based sacrificial inner core [44]. The inner core was filled with a PCL solution of 30% by hand squeezing it into the hollow spur of entirely ceramic scaffolds to both obtain greater resilience over hollow materials and enhanced the compressive stiffness.

5. Mechanical metamaterials for tissue engineering

The rapid growth and disruptive potential of 3D printing demand further research that both addresses the fundamental principles of 3D printing and likewise enables engineers to fully realize its potentials [150]. We can employ these capabilities to develop materials that derive some of their properties via their structural organizations rather than their intrinsic constituents. The need for advanced structures in tissue engineering demands a significant investment towards meta-biomaterials. The objectives of meta-biomaterials include incorporating multi-scale porosity at various length scales, improved strength-to-density ratio, energy-absorbing capacity, and self-assembly variation. We predict that bioprinting technologies coupled with novel approaches will cope with challenges in the design of printheads/nozzles, bioprinting resolution, and fabrication speed [23]. Another key challenge is to develop bioink formulations for creating tissue scaffolds and potential cell encapsulation [151,152]. Bioinks can be designed to mimic the extracellular matrix (ECM) in the target tissue or organ. The review of current bioinks can be found in the literature [153]. As a large portion of bioinks, natural-derived and synthetic hydrogels not only mimic the ECM but also offer printability and manufacturability of cell-laden structures. Hydrogels provide a hydrated environment and mechanical supports allowing hydrogel molecules to interact with each other in 3D and they promote cell attachment and proliferation [154]. They may include ECM clues for stem-like cell differentiation and regulation.

Some common examples of naturally-derived hydrogels are alginate, hyaluronic acid, gelatin, collagen I, fibrin, agarose, and basement membrane, while examples of

synthetically-derived hydrogels are polyethylene glycol and poloxamers [155]. One smart approach is to decellularize the natural tissue-specific ECM as a bioink solution for bioprinting of cell-laden structures. In one example of decellularization process, porcine cartilage, heart tissue excised from animals, and adipose tissue from the liposuction operation of donors were processed [156]. They encapsulated cells into ECM pre-gel and applied direct ink writing to create a cell-laden structure. They showed that the gene expression trends in the structures demonstrated an increase in the expression of tissue-specific markers over time in comparison with collagen and alginate.

Despite their cell-friendly environments, many hydrogels suffer from poor mechanical properties, degradation time and sometimes immune response by the host body [155]. To overcome shortcomings associated with poor mechanical properties, meta-biomaterials can offer practical solutions for tissue engineering applications. They can also enhance the cellular response towards tissue regeneration. In this section, we propose the use of the capabilities of 3D bioprinting and meta-biomaterials for significant advances in enhancing outcomes for patients (see the selected examples in Table 2).

5.1. Cartilage tissue engineering

Designing 3D hydrogel meta-biomaterials is a promising strategy for tuning mechanical signaling in bioreactor under cyclic loading conditions. Intrinsic pores at molecular scale in hydrogels naturally have a non-controllable stochastic arrangement. However, extrinsic pores can be precisely embedded by the emerging power of light-assisted 3D bioprinting, which can systematically distribute pores in hydrogel bioreactors [157]. Complex honeycomb-shaped structures were made of biocompatible hydrogels using photolithographic approaches [158]. Another example is a stereo-lithography-based device that has proved printability of cell-laden hydrogels [130]. The extrinsic or macroscopic architecture of a printed hydrogel using stereo-lithography can be designed to bear a range of pore sizes from ten microns up to the millimeter scale. The intrinsic structure of a hydrogel, however, consists of a stochastic spatial distribution of molecules connected through bonds of either covalent or ionic nature. The pores between molecules are usually micron or submicron sizes that host stem cells and their vital nutrients.

The mechanical properties of hydrogels in this perspective can be modulated through altering the type of bounds and the molecular weight, which affects the mobility of polymer chains. Recent studies have shown that covalently crosslinked hydrogels showed purely elastic behavior, while ionically crosslinked hydrogels showed notable stress relaxation or viscoelastic behavior that meaningfully affected cell spreading in 2D culture environments [159]. In the absence of ionic bonds, the type of generated mechanical loading in the hydrogel can play a significant role in the stem cell differentiation process. Cartilage tissues constantly bear cyclic hydrostatic pressure in natural body movements and this would be mimicked in an auxetic structure (Fig. 4). The auxetic deformation of articular cartilage scaffolds can lead to contractive deformation on lateral sides and this can impose a uniform hydrostatic pressure onto encapsulated cells. In a classical porous scaffold, uniaxial compression load is associated with volumetric expansion on lateral sides thus forcing the pore fluid to be evacuated from the scaffold volume. The fluid pressure *in vivo* is positive

outside the cartilage and this positive pressure confine the articular cartilages and preserves the pressure on the boundary [160].

5.2. Bone tissue engineering

Bone tissue, as a hierarchical structure over multiple length scales, has a non-mineralized organic component and a mineralized inorganic component [161]. The key requisites are extreme compressive strength and superior fracture toughness for any osteogenic biomaterials or scaffolds. The use of metamaterials based on light-assisted and extrusion-based 3D bioprinting would provide a wide range of choices of structures, from honeycomb to more complex models (Table 2). The use of biodegradable materials and inorganic phases makes it possible to access all 3D bioprinting modalities by using composite bioinks. Some biodegradable bioinks, such as PCL-based materials, are in the market with good potentials towards making functional meta-biomaterials.

For permanent implants, metallic structures can provide a cost-effective case. Titanium, stainless steel, and cobalt chrome alloys are the most appropriate alloys for bone implant applications [162]. However, metal 3D printing technology is not yet capable of creating production-grade metal parts that address the dimensional tolerance for such applications. We envision specific research into the application of biocompatible metals for patient-specific implants. The key issues with metallic implants involve both the surface roughness and internal imperfections made during the sintering process. To fully utilize the capacity of metallic metamaterials, it is critical to enable high process stability by improving implant quality. Higher stability of implants using theoretical structures indeed reduces their costs and the burden on the patients. Among different techniques, light-assisted AM can be used while considering the role of temperature. By a lower energy density, the temperature gradient mechanism is reduced, and the part quality could be increased. The potential of SLM/SLS will be tapped by enlarging the range of materials (Fig. 4). In the case of wrought and cast products, thermo-mechanical processing to create specific microstructure-property-performance linkages is a promising solution for product development of steels, aluminum alloys, and superalloys.

5.3. Skin tissue engineering

Human skin is composed of three heterogeneous layers: the epidermis, the dermis, and the hypodermis, the last of which is an extremely viscous and soft layer [163]. The dermis consists of a network of collagen with interspersed elastic fibers and lymphatic elements, all covered by an epidermal layer. This layer is partially filled by keratinized cells that are progressively dehydrated during their migration to the outer surface. Elastic fibers provide tissue toughness and hyperelasticity. Elastin, a known biomaterial for skin, comprises up to 70% of the dry weight in elastic ligaments and 2–4% in skin [164]. The next generation of dermis implants can include highly-elastic meta-biomaterials with the use of modern 3D bioprinting techniques or conventional molding, with elastin as a proper choice for degradable implants. The challenges in finding the optimum skin bioinks are both biocompatibility and proper degradation rate as resolution and other fabrication factors are not of any concerns in the case of superelastic models (Table 2).

5.4. Vascularized tissue engineering

Self-assembly is very promising for addressing the challenges related to vascularized tissues, such as hollow tubular tissue with (very) high resolutions and capillaries with variations along their length. This was highlighted by some self-folding structures, fabricated by DLP at micron-sized resolution, using a combination of methacrylated alginate and hyaluronic acid hydrogels [165]. Internal diameters of as low as 20 μm, comparable to that of small blood vessels, were achievable. Self-folded hydrogel-based structures support the survival of printed cells for at least seven days, and self-folding biocompatible polymers can be used in the fabrication of single or multilayered blood vessel models in complex organs such as the liver (Fig. 4). Self-folding biomaterials not only help control curvature for lumen formation but also provide dynamic environments for stimulating (i.e., sinusoidal contractions) endothelial cells to mimic *in vivo* like response.

Another solution is to apply 4D bioprinting for vascularized models by controlling the stimuli-responsive deformation and associated cell orientation in tissue models. They can respond to changes in temperature, pH, or chemical properties of the environment, enabling the release of desirable therapeutic agents such as macromolecular drugs or growth factors [150]. This approach requires proper selection of the vascular pattern, fabrication method, and bioink composition (Table 2). The choice of fabrication method is mainly limited to coaxial-nozzle extrusion-based AM for large vascular systems and high-resolution light-assisted AM, such as DLP and TPA, for capillaries. In both scenarios, there is a need for using sacrificial material as the material filling the channel model for very high-resolution structures. This time-dependent capacity of 4D bioprinting can offer unique functions in blood vessel models such as the release of biological factors for creating abnormal models (i.e., chemical programming) and a volumetric shrinking of capillaries for inducing mechanical stresses on the endothelial cells (i.e., physical programing).

5.5. Concluding remark

A future direction of biomaterials research involves the precise regulation of the underlying structure to achieve highly functional tissue models and biomimetic structures. This can lead to novel solutions for current challenges in the fabrication of meta-biomaterials. We have reviewed the current factors in the selection of fabrication methods and explained how advanced approaches can tackle the practical challenges in the fabrication of metamaterials. Another key challenge, which was not discussed here, is the selection of appropriate bioink compositions for any desired fabrication method, and this challenge may demand further study into both the chemistry and biology of bioinks. Indeed, bioink selection depends on the manufacturing process, the desired level of (biological) functionality, cost of production, and some other physiochemical factors. Discussion of these factors needs further investigation. We ultimately envision significant efforts for creating active synergy between the desired fabrication method and bioink composition. Future steps will involve adding time dependence to biomaterials towards 4D bioprinting.

Acknowledgements

A.K.M. acknowledges the receipt of R21DC018818 from National Institutes of Health and start-up funding from Rowan University. The authors thank **Prof. Wei Sun** (Department of Mechanical Engineering, Drexel University,

Philadelphia, USA) for his valuable feedback and comments for this manuscript, and they acknowledge **Dr. Hossein Goodarzi Hosseinabadi** (Department of Materials Engineering, Sharif University of Technology, Tehran, Iran) for his contributions in preparing the initial draft of this manuscript.

References

[1]. Kadic M, et al., Appl. Phys. Lett 101 (4) (2012) 049902

[2]. Lee SH, et al., J. Phys. Matter 21 (17) (2009) 175704

[3]. Bückmann T, et al., Adv. Mater 24 (20) (2012) 2710 [PubMed: 22495906]

[4]. Wegener M , Science 342 (6161) (2013) 939. [PubMed: 24264981]

[5]. Harris LD, J. Biomed. Mater. Res 42 (3) (1998).

[6]. Raghavan S , Rajeshkumar V, An overview of metamaterials in biomedical applications, in: PIERS Proceedings, 2013, p. 368.

[7]. Meza LR , et al. , in: Proceedings of the National Academy of Sciences, 112, 2015, p. 11502.

[8]. Lin CY, et al., J. Biomech 37 (5) (2004) 623. [PubMed: 15046991]

[9]. Lewis G, J. Mater. Sci 24 (10) (2013) 2293.

[10]. Chen VJ , Ma PX, Biomaterials 25 (11) (2004) 2065.

[11]. Yavari SA, et al., J. Mech. Behav. Biomed. Mater 43 (2015) 91 [PubMed: 25579495]

[12]. Deng Y , Kuiper J, Functional 3D Tissue Engineering Scaffolds: Materials, Technologies, and Applications, Woodhead Publishing, 2017

[13]. Zheng X, et al., Nat. Mater 15 (10) (2016) 1100 [PubMed: 27429209]

[14]. Haghpanah B, et al., Adv. Mater 28 (36) (2016) 7915 [PubMed: 27384125]

[15]. Miri AK , Voice J 28 (6) (2014) 657

[16]. Ritchie RO, Nat. Mater 10 (11) (2011) 817 [PubMed: 22020005]

[17]. Silver FH, et al., Skin Res. Technol 7 (1) (2001) 18 [PubMed: 11301636]

[18]. Hanif A, et al., ACS Appl. Mater. Interfaces (2018**))**

[19]. Hattori Y, et al., Adv. Healthc. Mater 3 (10) (2014) 1597. [PubMed: 24668927]

[20]. Kim D−H, et al., Science 333 (6044) (2011) 838. [PubMed: 21836009]

[21]. Jung Y, et al., Biomaterials 29 (35) (2008) 4630. [PubMed: 18804279]

[22]. Park YJ , Kim JK, Adv. Mater. Sci. Eng 2013 (2013) 5.

[23]. Miri AK, et al., Lab Chip 19 (11) (2019) 2019.

[24]. Kooistra GW, et al., J. Appl. Mech 74 (2) (2007).

[25]. O'NEIL J, et al., Deployable structures constructed from composite origami, in: Proceedings of the American Society for Composites—Thirty-third Technical Conference, 2018 .

[26]. Luz GM , Mano JF , Philosophical transactions of the royal society A: mathematical, Phys. Eng. Sci 367 (2009) 1587 1893 .

[27]. Callens SJ , Zadpoor AA, Mater. Today 21 (3) (2018) 241.

[28]. Saito K, et al., J. Intell. Mater. Syst. Struct 22 (9) (2011) 935.

[29]. Castle T, et al., Sci. Adv 2 (9) (2016) e1601258. [PubMed: 27679822]

[30]. Zhai J, et al., Thin-Walled Struct 145 (2019) 106356.

[31]. Neville RM, et al., Open shape morphing honeycombs through kirigami, ASME 2014 Conference on Smart Materials, Adaptive Structures and Intelligent Systems, American Society of Mechanical Engineers Digital Collection, 2014 .

[32]. Antolak-Dudka A, et al., Materials (Basel) 12 (2019) 1.

[33]. Zheng X, et al., Science (New York, N.Y.) 344 (6190) (2014) 1373.

[34]. Sun C, et al., Sensors Actuators A 121 (1) (2005) 113.

[35]. Behroodi E, et al., Sci. Rep 9 (1) (2019) 19692. [PubMed: 31873101]

[36]. Meza LR, et al., Science 345 (6202) (2014) 1322. [PubMed: 25214624]

[37]. Laumer T, et al., Phys. Procedia 39 (2012) 518.

[38]. Obata K, et al., Light 2 (12) (2013) e116.

[39]. Yuan S, et al., Adv. Mater. Technol**. (**2018)**.. (**

[40]. Farsari M , Chichkov BN, Nat. Photonics 3 (8) (2009) 450.
[41]. You S, et al., Addit. Manuf 30 (2019) 100834. [PubMed: 32832382]
[42]. Tumbleston JR, et al., Science 347 (6228) (2015) 1349. [PubMed: 25780246]
[43]. Wickeler AL , Naguib HE, Mater. Des 186 (2020) 108242.
[44]. Paredes C, et al., J. Eur. Ceram. Soc 39 (14) (2019) 4375.
[45]. Momeni K, et al., Mater. Des 183 (2019) 108124.
[46]. Yang H, et al., Compos. Struct 214 (2019).
[47]. Kenel C, et al., Nat. Commun 10 (1) (2019) 904. [PubMed: 30796218]
[48]. Skylar-Scott MA, et al., Nature 575 (7782) (2019) 330. [PubMed: 31723289]
[49]. Yoon YJ, et al., Development of three-nozzle extrusion system for conformal multi-resolution 3d printing with a robotic manipulator, ASME 2019 International Design Engineering Technical Conferences and Computers and Information in Engineering Conference, American Society of Mechanical Engineers Digital Collection, 2019 .
[50]. Chan N , Evans K, J. Mater. Sci 32 (22) (1997) 5945.
[51]. Mohsenizadeh S, et al., Physica Status Solidi 256 (10) (2019) 1800587.
[52]. Alderson K, et al., Plastics Rubber Compos. 31 (8) (2002) 344.
[53]. Alderson K, et al., physica status solidi 242 (3) (2005) 509.
[54]. Evans K , Caddock B , Phys J. D Appl. Phys 22 (12) (1989) 1883.
[55]. Friis E, et al., J. Mater. Sci 23 (12) (1988) 4406.
[56]. Choi J , Lakes R, J. Mater. Sci 27 (19) (1992) 5375.
[57]. Milton GW, J. Mech. Phys. Solids 40 (5) (1992) 1105.
[58]. Geng LC, et al., Exp. Mech. (2019).
[59]. Zheng X, et al., Nat. Mater 15 (10) (2016) 1100. [PubMed: 27429209]
[60]. Ding Y , Kovacevic R, JOM 68 (7) (2016) 1774.
[61]. Zhang W, et al., Adv. Funct. Mater 23 (25) (2013).
[62]. Pandini S, et al., Mech. Res. Commun 103 (2020) 103463.
[63]. Yuan S, et al., Mater. Des 120 (2017) 317.
[64]. Chen D , Zheng X, Sci. Rep 8 (1) (2018) 9139. [PubMed: 29904093]
[65]. Mirzaali MJ, et al., Sci. Rep 8 (1) (2018) 965. [PubMed: 29343772]
[66]. Wang K, et al., Mater. Des 67 (2015) 159.
[67]. Lakes R, Science (1987) 1038.
[68]. Mohsenizadeh M, et al., Mater. Des 139 (2018) 521.
[69]. Bodaghi M, et al., Mater. Des 131 (2017) 81.
[70]. Simpson B, et al., J. Mater. Chem 20 (17) (2010) 3496.
[71]. Felton SM, et al., Soft Matter 9 (32) (2013) 7688.
[72]. Liu Y, et al., Soft Matter 8 (6) (2012) 1764.
[73]. Luo X , Mather PT, Macromolecules 42 (19) (2009) 7251.
[74]. Qiu Y , Park K, Adv. Drug Deliv. Rev 53 (3) (2001) 321. [PubMed: 11744175]
[75]. Zarek M, et al., Adv. Mater 28 (22) (2016) 4449. [PubMed: 26402320]
[76]. Sadeqi A, et al., Microsyst. Nanoeng 5 (1) (2019) 16. [PubMed: 31057943]
[77]. Ge Q, et al., Sci. Rep 6 (1) (2016) 31110. [PubMed: 27499417]
[78]. Huang B, et al., Carbohydr. Polym 231 (2020) 115736. [PubMed: 31888822]
[79]. Kim Y, et al., Nature 558 (7709) (2018) 274. [PubMed: 29899476]
[80]. Chen Y, et al., Mater. Des 190 (2020) 108567.
[81]. Bodaghi M, et al., Materials (Basel) 12 (8) (2019) 1353.
[82]. Garcia C, et al., Progr. Electromagn. Res. Lett 34 (2012) 75.
[83]. Cornock R, et al., Biofabrication 6 (2) (2014) 025002. [PubMed: 24658021]
[84]. Bodaghi M, et al., Smart Mater. Struct 25 (10) (2016) 105034.
[85]. Barthelat F , Rabiei R, J. Mech. Phys. Solids 59 (4) (2011) 829.

[86]. Ledbetter HM , Reed RP, J. Phys. Chem. Reference Data 2 (3) (1973) 531.
[87]. Ajdari A, et al., Int. J. Solids Struct 49 (11–12) (2012) 1413.
[88]. Zhang Z, et al., in Proceedings of the Royal Society B: Biological Sciences, 278, 2011, p. 519 1705 .
[89]. Schaedler TA, et al., Science 334 (6058) (2011) 962. [PubMed: 22096194]
[90]. Rayneau-Kirkhope D, et al., Phys. Rev. Lett 109 (20) (2012) 204301. [PubMed: 23215491]
[91]. Rahman KM, et al., J. Manuf. Sci. Eng 140 (1) (2018).
[92]. Naik S, et al., A review on various aspects of auxetic materials, in: AIP Conference Proceedings, 2105, AIP Publishing LLC, 2019 .
[93]. Alderson K , Evans K, Polymer (Guildf) 33 (20) (1992) 4435.
[94]. Pickles A, et al., Polym. Eng. Sci 36 (5) (1996) 636.
[95]. Alderson K, et al., J. Mater. Sci. Lett 17 (16) (1998) 1415.
[96]. Lakes R, Science 235 (4792) (1987) 1038. [PubMed: 17782252]
[97]. Liu F , Urban MW, Prog. Polym. Sci 35 (1–2) (2010) 3.
[98]. Klavins E, IEEE Control Syst. Mag 27 (4) (2007) 43.
[99]. Zhao Q, et al., Prog. Polym. Sci 49 (2015) 79.
[100]. Sahasrabudhe H, et al., Chapter 17 - Laser-based additive manufacturing processes, in: Lawrence J (Ed.), Advances in Laser Materials Processing (Second Edition), Woodhead Publishing, 2018, p. 507.
[101]. Gu D , Laser Additive Manufacturing (AM): classification, processing philosophy, and metallurgical mechanisms, in: Laser Additive Manufacturing of High--Performance Materials, Springer Berlin Heidelberg, Berlin, Heidelberg, 2015, p. 15.
[102]. Vyatskikh A, et al., Nat. Commun 9 (1) (2018) 593. [PubMed: 29426947]
[103]. Kumar S , Kruth JP, Mater. Des 31 (2) (2010) 850.
[104]. Kumar S , Pityana S, Adv. Mater. Res 227 (2011) 92.
[105]. Santos EC, et al., Int. J. Mach. Tools Manuf 46 (12) (2006) 1459.
[106]. Amir M, et al., Biofabrication (2019).
[107]. Mao M, et al., Micromachines (Basel) 8 (2017) 113.
[108]. Sakellari I, et al., Adv. Opt. Mater 5 (16) (2017) 1700200.
[109]. Maruo S , Fourkas JT, Laser Photonics Rev. 2 (1–2) (2008) 100.
[110]. Muller N, et al., Adv. Opt. Mater 2 (2) (2014) 115.
[111]. Gansel JK, et al., Appl. Phys. Lett 100 (10) (2012) 101109.
[112]. Zhou X, et al., AIP Adv 5 (3) (2015) 030701.
[113]. Bertoldi K, et al., Nat. Rev 2 (2017) 17066.
[114]. Surjadi JU, et al., Adv. Eng. Mater 21 (3) (2019) 1800864.
[115]. Wang C−Y , et al. , in: Proceedings of the Institution of Mechanical Engineers, Part C: Journal of Mechanical Engineering Science, 232, 2018, p. 2998.
[116]. Eckel ZC, et al., Science 351 (6268) (2016) 58. [PubMed: 26721993]
[117]. Frazier WE, J. Mater. Eng. Perform 23 (6) (2014) 1917.
[118]. Agarwala M, Rapid Prototyp. J 1 (1) (1995) 26.
[119]. Lee H, et al., Int. J. Precis. Eng. Manuf.-Green Technol 4 (3) (2017) 307.
[120]. Yap CY, et al., Appl. Phys. Rev 2 (2015) 041101.
[121]. Balla VK, et al., Int. J. Appl. Ceram. Technol 5 (3) (2008) 234.
[122]. Rahmati S, et al., 10.12 - direct rapid tooling, in: Hashmi S, et al. (Eds.), Comprehensive Materials Processing, Elsevier, Oxford, 2014, p. 303.
[123]. Liu Z, et al., Int. J. Adv. Manuf. Technol 102 (1) (2019) 969.
[124]. Ning F, et al., Rapid Prototyp. J (2019).
[125]. Ziętala M, et al., Mater. Sci. Eng. A 677 (2016) 1.
[126]. Hull CW, Apparatus for production of three-dimensional objects by stereolithography. USA, (1984)

[127]. Lu Y, et al., J. Biomed. Mater. Res. A 77 (2) (2006) 396. [PubMed: 16444679]
[128]. Kadry H, et al., Eur. J. Pharmaceut. Sci 135 (2019) 60.
[129]. Schönberger M , Hoffstetter M , 4 - Generative manufacturing technologies—the future?, in: Schönberger M, Hoffstetter M **(Eds.)** Emerging Trends in Medical Plastic Engineering and Manufacturing, William Andrew Publishing, 2016, p. 107.**(Eds.)**
[130]. Miri Amir K, et al., Adv. Mater 30 (27) (2018) 1800242.
[131]. Maciulaitis J, et al., Biofabrication 7 (1) (2015) 015015. [PubMed: 25797444]
[132]. Torgersen J, et al., Adv. Funct. Mater 23 (36) (2013) 4542.
[133]. Skylar-Scott MA, et al., Adv. Healthc. Mater 5 (10) (2016) 1233. [PubMed: 27059425]
[134]. Xing JF, et al., Chem. Soc. Rev 44 (15) (2015) 5031. [PubMed: 25992492]
[135]. You S, et al., J. Mater. Chem. B 6 (15) (2018) 2187. [PubMed: 30319779]
[136]. Bauer S, et al., Adv. Mater 26 (1) (2014) 149. [PubMed: 24307641]
[137]. Janusziewicz R , et al. , in: Proceedings of the National Academy of Sciences of the United States of America, 113, 2016.
[138]. Travitzky N, et al., Adv. Eng. Mater 16 (6) (2014) 729.
[139]. Hess AJ, et al., ACS Omega 4 (24) (2019) 20558. [PubMed: 31858040]
[140]. Ali MH, et al., Int. J. Adv. Manuf. Technol 86 (1–4) (2016) 999.
[141]. Abilgaziyev A, et al., Design and development of multi-nozzle extrusion system for 3D printer, in: 2015 International Conference on Informatics, Electronics & Vision (ICIEV), IEEE, 2015, p. 1.
[142]. Sitthi-Amorn P, et al., in MultiFab: a Machine Vision Assisted Platform For Multi-Material 3D Printing, Association for Computing Machinery, 2015, p. 129.
[143]. Dong Y , et al. , in: Fabricating Spatially-Varying Subsurface Scattering, Association for Computing Machinery, 2010, p. 62.
[144]. Ning L , Chen X, Biotechnol. J 12 (8) (2017) 1600671.
[145]. Tan EYS , Yeong WY, Int. J. Bioprinting 1 (1) (2015).
[146]. Hardin JO, et al., Adv. Mater 27 (21) (2015) 3279. [PubMed: 25885762]
[147]. Liu W, et al., Adv. Mater 29 (3) (2017) 1604630.
[148]. Vancauwenberghe V, et al., J. Food Eng 225 (2018) 42.
[149]. Surjadi JU, et al., Adv. Eng. Mater 21 (3) (2019) 1800864.
[150]. Miri AK, et al., Biomaterials 198 (2019) 204. [PubMed: 30244825]
[151]. Ji S , Guvendiren M, Front. Bioeng. Biotechnol 5 (2017).
[152]. Miri A, et al., Biofabrication (2019).
[153]. Hölzl K, et al., Biofabrication 8 (3) (2016) 032002. [PubMed: 27658612]
[154]. Jungst T, et al., Chem. Rev 116 (3) (2016) 1496. [PubMed: 26492834]
[155]. Merceron TK , Murphy SV ,Chapter 14 - hydrogels for 3D bioprinting applications, in: Atala A, Yoo JJ **(Eds.),** Essentials of 3D Biofabrication and Translation, Academic Press, Boston, 2015, p. 249.**(Eds.),**
[156]. Pati F, et al., Nat. Commun 5 (1) (2014) 3935. [PubMed: 24887553]
[157]. Miri AK, et al., Acta Biomater. (2018).
[158]. Soman P, et al., Soft Matter 8 (18) (2012) 4946. [PubMed: 24014252]
[159]. Chaudhuri O, et al., Nat. Mater 15 (3) (2016) 326. [PubMed: 26618884]
[160]. Bhosale AM , Richardson JB, Br. Med. Bull 87 (1) (2008) 77. [PubMed: 18676397]
[161]. Miri AK, et al., Biomaterials 85 (2016) 128. [PubMed: 26871889]
[162]. Seyyedhosseinzadeh H, et al., Joint Bone Sci. J 2 (1) (2014) 67.
[163]. Groeber F, et al., Adv. Drug Deliv. Rev 63 (4–5) (2011) 352. [PubMed: 21241756]
[164]. Ayad S, et al., The Extracellular Matrix Factsbook, Elsevier, 1998 .
[165]. Kirillova A, et al., Adv. Mater 29 (46) (2017) 1703443.
[166]. Li Y, Zeng C, Polymer 87 (2016).

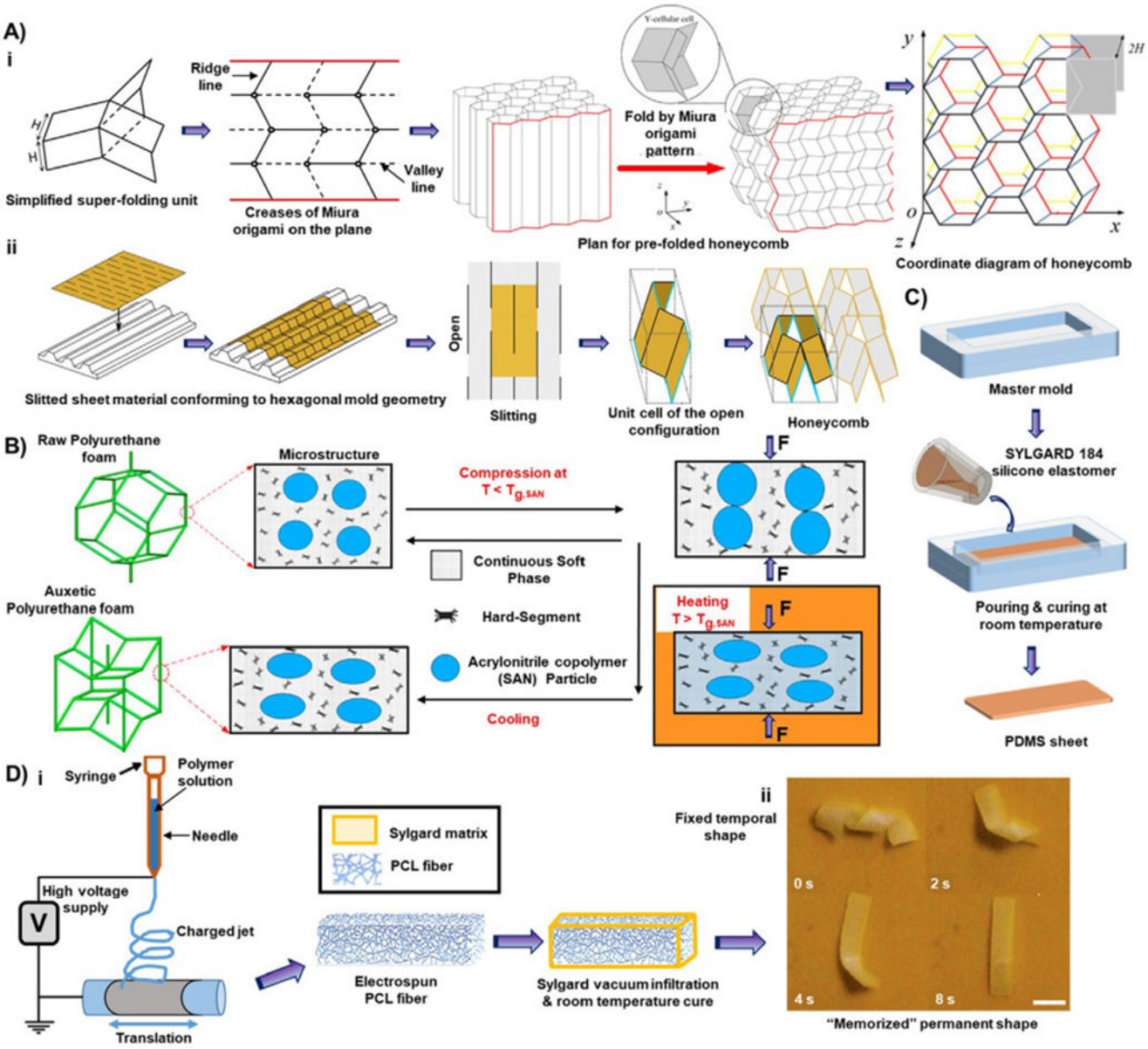

Fig. 1.

Conventional methods for metamaterials: A) Ultra-stiff material: (i) Miura origami folding technique for honeycomb construction [30], (ii) Kirigami technique for open honeycomb construction by converting a 2D sheet into a 3D cellular structure [31]; B) Auxetic material: the process of fabrication of auxetic foam through molding [166]; C) Super-elastic material: casting of PDMS in master mold and room temperature curing; D) (i) Self-assembly and programmable material: two-step fabrication using electrospinning of PCL fiber and Sylgard vacuum infiltration, (ii) photographs of Sylgard/PCL composite showing the recovery from a fixed temporary shape to its memorized permanent shape on a temperature-controlled plate at 80 °C (the scale bar is 5 mm) [73]. *Reprinted and modified by permission of Elsevier, American Society of Mechanical Engineers, and Royal Society of Chemistry.*

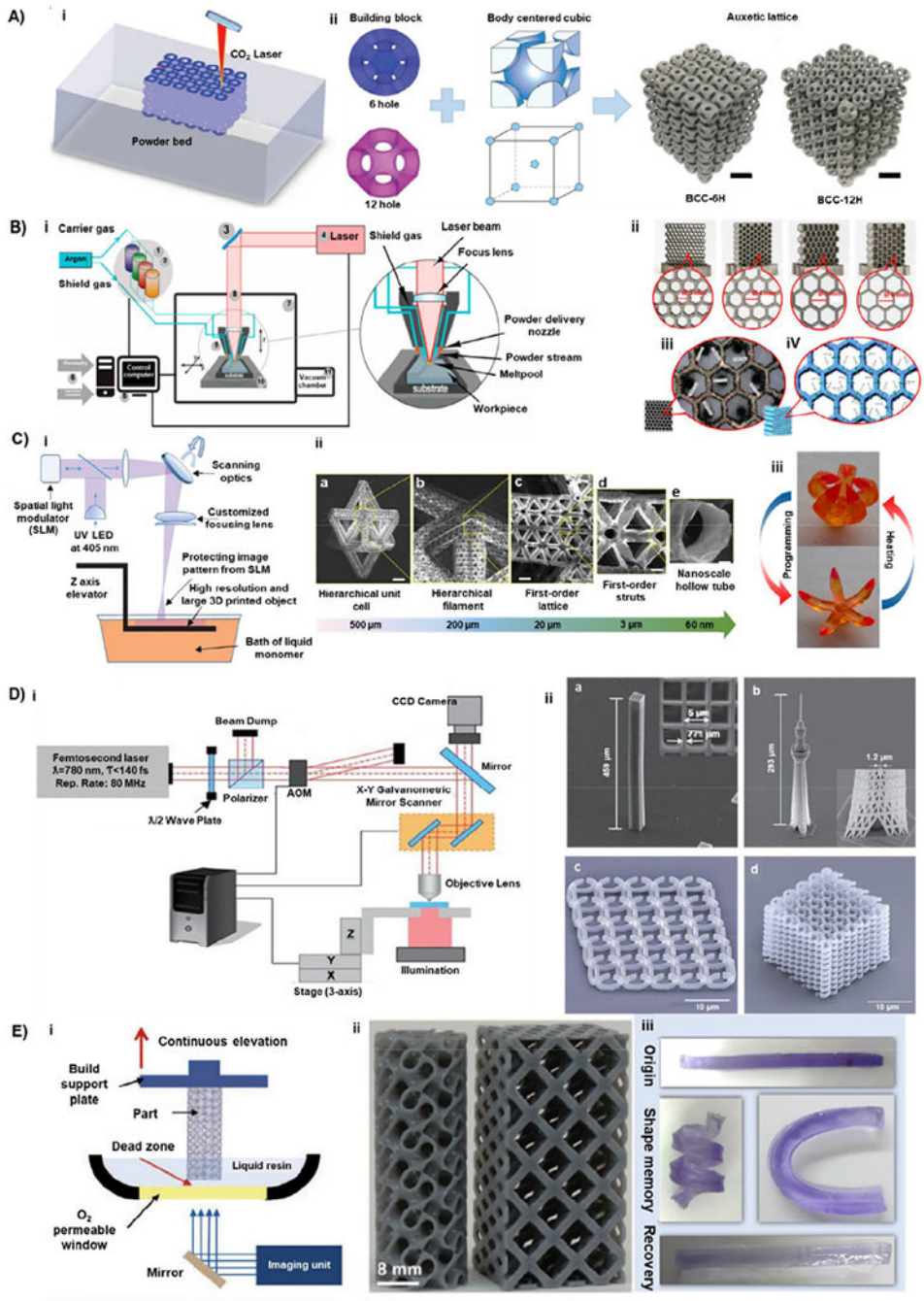

Fig. 2.

Light-assisted AM: A) (i) Schematic illustration of a typical building platform for SLS process, (ii) illustration of the concept of structural designs of BCC-6H and BCC-12H metamaterials (Scale bar is 10 mm)[39]; B) (i) Schematic illustration of the LENS system, (ii) four variants of Ti6Al4V thin-walled honeycomb structures with different the unit cell size, (iii) with the application of optical microscopy, and (iv) a 3D model reconstructed from CT data;[32] C) (i) Schematic illustration of large area projection micro-stereolithography, (ii) (a-e) scanning electron micrographs showing cross-section breakdown of structural

hierarchy of the multi-scale metamaterial unit cell. (scale bars are 10 and 3 μm in c [13] and (iii) the demonstration of the transition between as printed shape and temporary shape of multi-material shape memory grippers [77]; D) (i) Schematic illustration of TPA, (ii) (a,b) scanning electron micrographs of 6 × 6 grid structure "Tokyo Skytree" fabricated by TPA with 100×high-magnification microscope objective [38] (c,d) a 3D split-ring metamaterial structure, fabricated using a metal-binding hybrid polymer composite. TPA is the only technology that can be used for the fabrication of 3D free-standing structures with submicrometric resolution [40]; E) (i) Schematic demonstration of CLIP method. The oxygen-permeable window creates a dead zone (persistent liquid interface) between the build part and the window, (ii) a gyroid (left) and an argyle (right), printed at a speed of 500 mm/hour [42], (iii) associated shape memory effect [78]. *Reprinted and modified by permission of John Wiley and Sons*, *Multidisciplinary Digital Publishing Institute*, *Springer Nature*, *The American Association for the Advancement of Science*, *and Elsevier*.

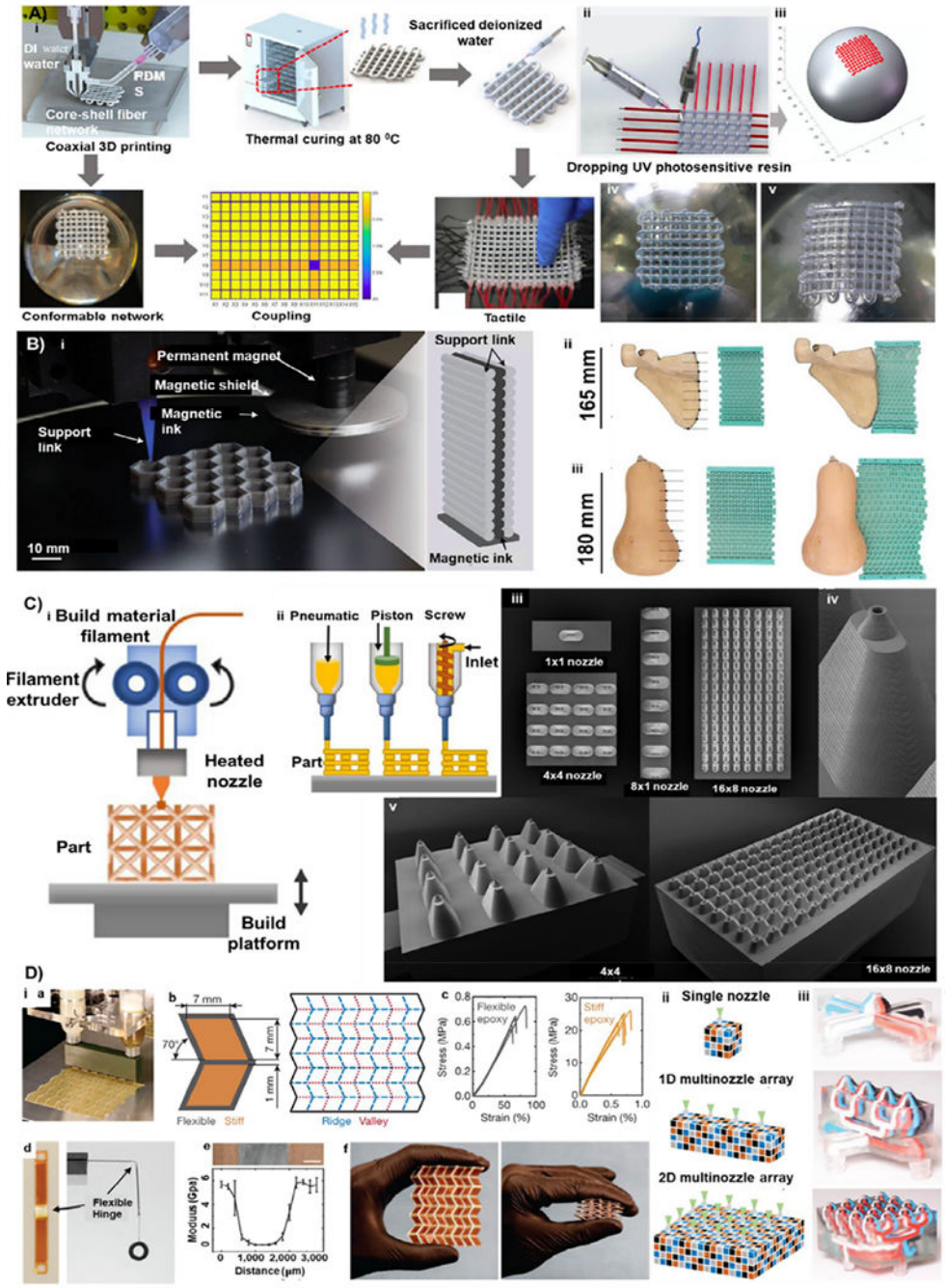

Fig. 3.

Nozzle-based AM: A) (i) Coaxial drawing for preparation of a core-shell fiber-based tactile sensor, (ii) conformal manufacturing model, (iii) path planning for printing on a ball, and printed sensor array (iv) DI water and PDMS, or (v) liquid metal and PDMS [80]; B) (i) 3D Printing multilayered hexagonal arrays using magnetic and support inks [79], matching the shapes of three real objects including an anatomical model of (ii) scapula and (iii) a pumpkin [65]; C) (i) The basic working principle and setup for FDM [149], (ii) micrographs of different nozzle arrays for two-material 3D printing, (iii) magnified micrograph of the

printheads (scale bar is 200 μm), (iv) micrographs of other printheads [48]; D) (i) Miura pattern using (a) two material printhead, along with (b) Miura folding pattern and (c) mechanical data for flexible epoxies, (d) cantilevers a hinge demonstrate patterned bending and the (e) an interfacial region (scale bar is 500 μm), (f) folding behavior; (ii) voxelated architectures printed using single (0D) nozzle, multi-nozzle (1D, 2D) systems, and (iii) corresponding four-material printheads [48]. *Reprinted and modified by permission of Elsevier*, *Springer Nature*, *and John Wiley and Sons*.

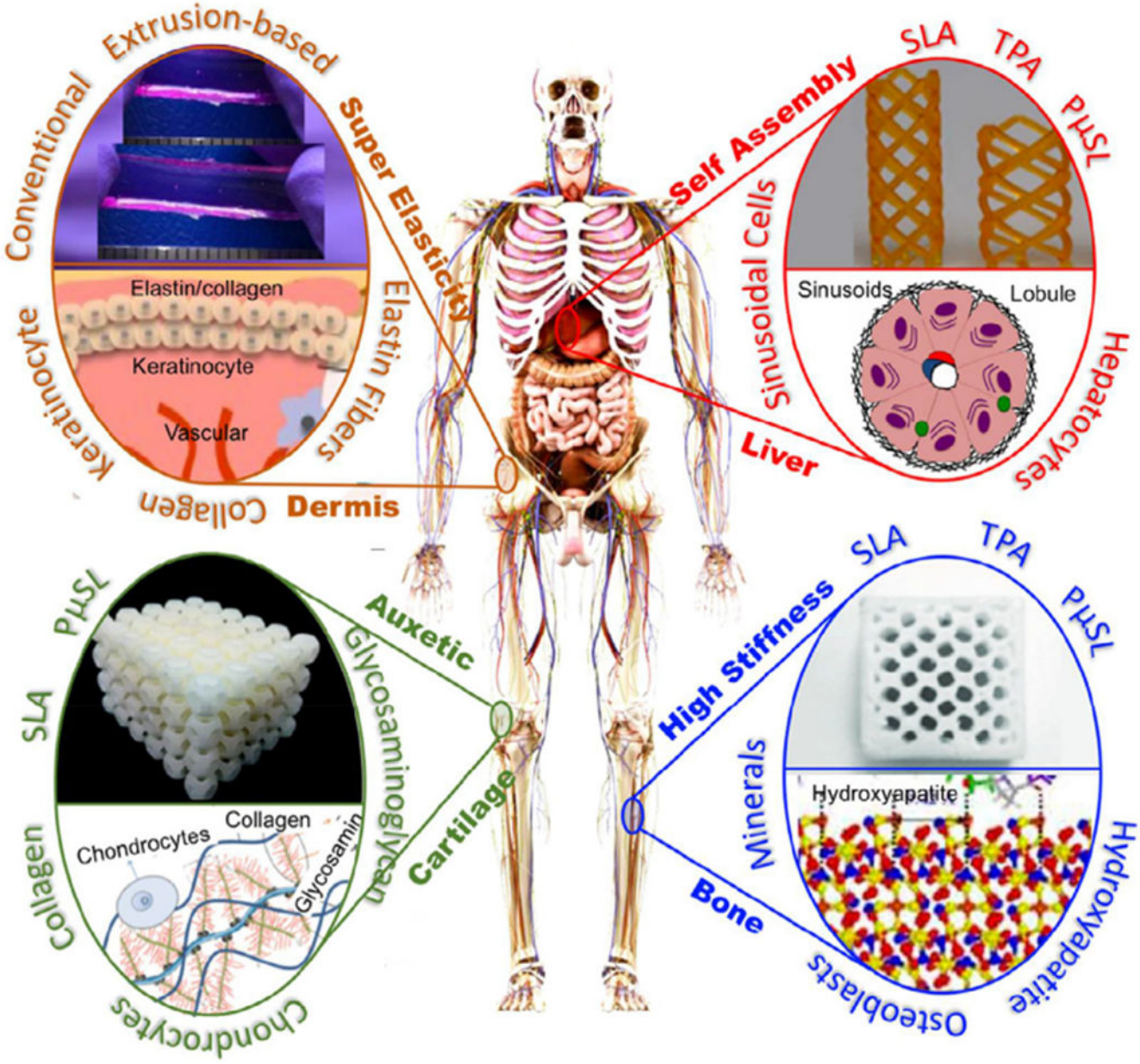

Fig. 4.

Proposed meta-biomaterials: An overview of proposed mechanical meta-biomaterials for four different organs in tissue engineering and regenerative medicine: superelastic models for dermis/skin tissue, auxetic models for articular cartilage, self-assembly models for liver, and high-stiff models for cortical bone tissue.

Table 1

Selected mechanical metamaterials and their fabrication methods.

Function	Material	Method	Fabrication Challenges	References
Ultra-stiffness (high stiffness-to-weight ratio)	Metals, polymers, composites	Conventional	Time-consuming process for material handling, lack of repeatability, product uncertainties, making small structures	[24–31]
	Polymers, metals, ceramics, nanocomposites	Light-assisted AM	Pre-processing to make material compositions, local imperfections for polymers and metals, surface imperfections	[13,32–42]
	Polymers, composites	Extrusion-based AM	Instability of structure, the anisotropy of structure	[43–49],
Negative-Poisson's ratio	Polymers, metals	Conventional	Lack of complexity, absence of automation for periodic structures	[50–57,166]
	Metals, polymers, composites	Light-assisted AM	Desired material compositions, light scattering for internal spaces/pores,	[58–64]
	Polymers	Extrusion-based AM	Low resolution in structures, Instability among layers in structures	[48,49,65,66]
High-toughness & super elasticity	Polymers	Conventional	Limited selection of materials, lack of a flexible and versatile platform, low mass, negative mass density	[54–67]
	Polymers, metals	Light-assisted AM	Inhomogeneity in structures, high resolution, and large-scale parts	[13,38,68]
	Polymers	Extrusion-based AM	Multi-stability, a separation between layers, multi-scale fabrication,	[65,69]
Self-assembly & programmable	Shape memory polymers	Conventional	Complexity in design, misalignment, lack of control in patterns	[70–74]
	Shape memory metals/polymers, composites	Light-assisted AM	Material composition, opacity requirement for complex materials, post-processing to activate the structure	[59,62,75–78]
	Shape memory composi-tes, Shape memory polymers, composites	Extrusion-based AM	Complexity of structures, multi-material fabrication for products, incorporation of architecture, size effects	[79–84]

Table 2

Proposed fabrication methods for tissue scaffold meta-biomaterials.

Target	Desired Function/Range	Biomaterials/Bioinks Composition	Proposed Fabrication	Fabrication Challenge
Articular cartilage	Anisotropic and auxetic deformation (Poisson's ratio <0)	Chondrocyte/stem-cell laden natural hydrogels (collagen gel) or polymers	SLA-based AM DLP-based AM	Stability, flexibility Stability, resolution
Cortical bone	Extreme stiffness/high toughness (elastic modulus > 100 MPa; strength > 500 MPa)	Osteoblast/stem-cell laden natural hydrogels or polymers, acellular metals, ceramics/phosphate paste	Nozzle-based AM Nozzle-based AM NLS-based AM, SLS/SLM-based AM	Speed, composition Strength, speed, fidelity Surface properties (porosity)
Dermis	Super-elasticity (total strains > 100%)	Natural hydrogels or polymers loaded with/without keratinocytes	Conventional, nozzle-based AM	Mold precision, ink selection
Blood vessels	Time-based volume variations (4D printing; self-assembly)	Natural hydrogels or soft polymers seeded by endothelial cells	DLP/TPA-based AM DLP-based AM	Repeatability, assembly Fabrication resolution